Molecular Crystals and Liquid Crystals
Publication details, including instructions for authors and subscription information:
http://www.tandfonline.com/loi/gmcl20

Identifying the Magnetic Phases on Annealed Amorphous Alloys Using Forc Diagrams

R. Lavín [a b], B. Torres [a], D. Serafini [a] & J. C. Denardin [a c]

[a] Departamento de Física, Universidad de Santiago de Chile, Santiago, Chile

[b] Facultad de Ingeniería, Universidad Diego Portales, Santiago, Chile

[c] Centro para el Desarrollo de la Nanociencia y Nanotecnología, Santiago, Chile

Version of record first published: 28 May 2010

To cite this article: R. Lavín, B. Torres, D. Serafini & J. C. Denardin (2010): Identifying the Magnetic Phases on Annealed Amorphous Alloys Using Forc Diagrams, Molecular Crystals and Liquid Crystals, 521:1, 279-287

To link to this article: http://dx.doi.org/10.1080/15421401003715835

Mol. Cryst. Liq. Cryst., Vol. 521: pp. 279–287, 2010

ISSN: 1542-1406 print/1563-5287 online
DOI: 10.1080/15421401003715835

Taylor & Francis
Taylor & Francis Group

Identifying the Magnetic Phases on Annealed Amorphous Alloys Using Forc Diagrams

R. LAVÍN,[1,2] B. TORRES,[1] D. SERAFINI,[1] AND J. C. DENARDIN[1,3]

[1]Departamento de Física, Universidad de Santiago de Chile, Santiago, Chile
[2]Facultad de Ingeniería, Universidad Diego Portales, Santiago, Chile
[3]Centro para el Desarrollo de la Nanociencia y Nanotecnología, Santiago, Chile

Results of thermal annealing on $Fe_{66}Co_{18}B_{15}Si_1$ amorphous alloy by means of linear heating and isothermal process are presented. The analysis of the DSC curve and X-ray diffraction of the annealed samples indicate the synthesis of magnetic nanocrystals in the Fe_7Co_3 phase, and the co-existence of two coupled magnetic phases; one soft magnetic phase due to the remaining amorphous matrix and a hard magnetic phase associated to the crystalline nanoparticles. The presence of these different magnetic phases and their coupling are unhidden by analysis of FORC diagrams of the samples.

Keywords Amorphous alloy; annealing; forc diagram; magnetic properties

Introduction

Nanocrystalline materials that display high permeability and low coercivities have been absorbing growing attention from the scientific community, not only because their potential use in technological applications, but also because they provide an excellent setting to study basic problems in magnetism [1]. Nanocrystalline materials obtained from the controlled devitrification of amorphous ferromagnetic ribbons present, even at the initial stages of nanocrystallization, coexistance of different magnetic phases. The possibility to easily modify the size distribution and relative volume fraction of the crystallites through annealing makes of this nanostructured materials an ideal environment to investigate interactions among magnetic particles [2–5], surface effects [6], superparamagnetism [7], and several new phenomena that emerged with the reduced dimensions of the crystallites.

The most common method to investigate the magnetic properties of these systems is the measurement of hysteresis curves. However, the analysis of these curves usually is not enough to clarify all the main aspects of more complex systems.

Address correspondence to R. Lavín, Facultad de Ingeniería, Universidad Diego Portales, Ejército 441, Santiago, Chile. Tel.: 56-2-6762418; Fax: 56-2-6762402; E-mail: roberto.lavin@udp.cl

The FORC diagrams can be a useful tool to study coexistence of different reversion modes in arrays of nanodots [8,9], identify magnetic phases in annealed alloys [10], study dipolar interactions between magnetic nanostructures [11,12] and quantify the amount of reversible magnetization of the system as a function of the amount of irreversible magnetization [13].

In this paper the FORC diagrams are used to investigate in detail the magnetic properties in samples of $Fe_{66}Co_{18}B_{15}Si_1$ annealed at temperatures above the crystallization.

Experimental

Amorphous ribbons with composition of $Fe_{66}Co_{18}B_{15}Si_1$, produced by melt-spinning, have been submitted to linear thermal annealing in a DSC-TGA 2960 TA-Instruments oven, on a nitrogen atmosphere. Samples were heated from ambient temperature to different final temperatures $T_f = 833$, 953, 1053, and 1153 K at a heating rate of 20 K/min. In order to characterize the crystallization process, isothermal and non-isothermal curves have been measured. X-ray Bragg diffractions were measured on a Shimadzu XRD 6000 with Cu anode. Magnetic measurements were performed by a homemade alternating gradient magnetometer (AGM), at room temperature and with the plane of the alloys parallel to the field.

Results and Analysis

Figure 1 shows the DSC curve for the $Fe_{66}Co_{18}B_{15}Si_1$ sample submitted to a lineal heating at a rate of 20 K/min, from 300 K to 1153 K. The final annealing temperatures for the different samples that appear in this work are displayed in the curve. Two exothermal processes are observed in this figure, the first one at 703 K and the second one at 788 K.

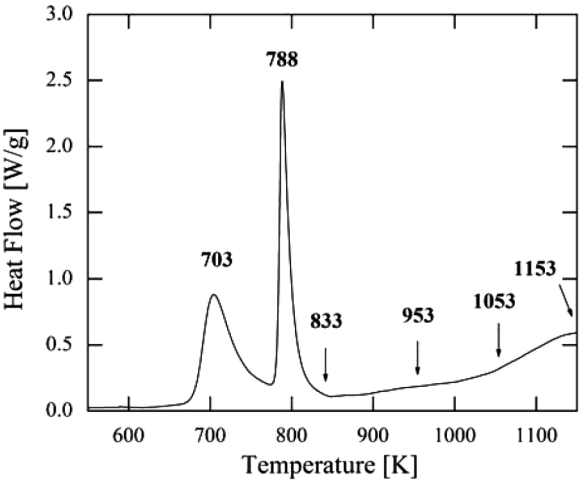

Figure 1. DSC scan at 20 K/min for the $Fe_{66}Co_{18}B_{15}Si_1$ sample. The arrows indicate the points up to where each sample was treated ($T_f = 833$, 953, 1053, and 1153 K) and the two exothermal process at 703 and 788 K described in the text.

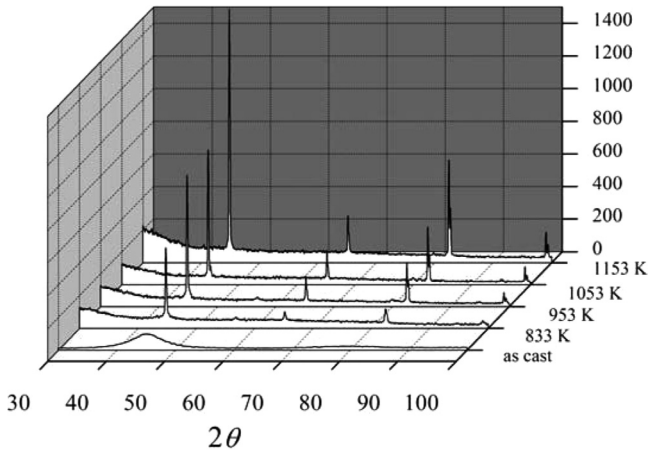

Figure 2. X-ray diffraction spectra for the as-cast sample and the sample annealed up to different final temperatures.

In order to investigate the origin of the two peaks at 703 K and 788 K, an isothermal process (not shown here) has been fitted by a Johnson–Mehl–Avrami [15,16] equation, and the linear DSC curve was analyzed by a modified Kissinger–Ozawa [15] model. This analysis indicates that the peak at 703 K is due to an increase of the preexistent Fe_7Co_3 grains and the peak at 788 K corresponds to the nucleation of new Fe_7Co_3 crystallites.

Figure 2 shows the X-ray spectra for the as-cast sample and the annealed samples. From these curves it is possible to observe a clear increase of the peak at 2θ corresponding to the Fe_7Co_3 phase. The first X-ray spectra correspond to the as cast sample. X-ray diffractions for the annealed samples, with different final annealing temperatures T_f, show a clear evolution of the peaks corresponding to the crystalline Fe_7Co_3 phase. Final temperatures $T_f = 833$, 953, 1053, and 1153 K shown here corresponds to annealing temperatures higher than the temperature of the second exothermal peak, at 788 K, observed in the DSC analysis. This means that the increase in height of the X-ray diffraction peaks shown in Figure 2 is due to increase of the size of the crystallites. Table 1 shows the results of the average size of crystallites as function of T_f obtained by the Scherrer formula [17]. From the table one can observe that the size of grains increase up to 1053 K, and then decrease for 1153 K. This can be explained by an anomalous growing of the crystallites at very high temperatures [18]. In this table are also shown the lattice constants, which are in good agreement with the one for Fe_7Co_3 phase, that are $\alpha = 2.863$ Å [19].

Table 1. Fe_7Co_3 crystal sizes, obtained using the Scherrer formula, and lattice constants of the annealed samples

T_f (K)	Crystal sizes (nm)	Lattice constant (Å)
833	45.53	2.8637
953	74.75	2.8657
1053	104.6	2.8662
1153	86.45	2.8668

In order to have a more detailed picture of the evolution of the structure of the ribbons with annealing, we have performed a detailed magnetic characterization of the samples by means of FORC curves and diagrams.

The measurement of a FORC curve starts by saturating the sample at a large positive applied field. Then the field is decreased to a reversal field H_a. The FORC is defined as the magnetization curve that results when the applied field is increased from H_a back to saturation. The magnetization at the applied field H_b on the FORC with reversal point H_a is denoted by $M(H_a, H_b)$, where $H_b > H_a$.

A statistical model that describes the system as a set of magnetic entities (hysterons) based on the Preisach model [14,20] is used to illustrate and obtain information from the FORC. The extended probability density function (pdf) of the ensemble is defined by [21,22]

$$\rho(H_a, H_b) = -\frac{1}{2}\frac{\partial^2 M}{\partial H_a \partial H_b}. \quad (1)$$

This function extends over the entire plane H_a, H_b. A FORC diagram is a contour plot of the pdf (Eq. (1)), and can be presented in terms of the variables $H_c = (H_b - H_a)/2$ and $H_i = (H_b + H_a)/2$ which are the fields of switching (coercivity of hysteron) and interaction (bias of each hysteron) [21], allowing to capture the reversible component of the magnetization, which appears focused on $H_c = 0$. The pdf (Eq. (1)) of a sample is obtained by numerically derivation of $M(H_a, H_b)$, which contains all FORC measurements. The FORC diagram is obtained performing the contour plot of the pdf (Eq. (1)).

Figure 3 shows the FORC curves for samples annealed at different temperatures. The major hysteresis loops, delineated by the outer boundaries of the FORC's, correspond exactly to the hysteresis curves of each sample, and exhibit only subtle differences.

While the hysteresis curve of the as-cast sample (not shown here) is typical of an amorphous soft material, with coercivity close to zero, the curves for annealed samples show higher coercivities as T_f increases. This is a clear indicative of the formation of small, monodomain, Fe_7Co_3 crystals, which increase their size as T_f increases.

The hysteresis curves of the samples annealed at temperatures above $T_f = 953$ K is a waist loop, and the waist features are more symmetrically centered around $M = 0$ for samples treated at higher temperatures. This type of waist loop have been observed in different materials and is associated to the presence of two magnetic phases, a hard magnetic phase and a soft magnetic phase, that are coupled [23–29]. Waist loops have been also investigated by theoretical works [30–32], and is associated to an antiferromagnetic coupling between the nanoparticles of the hard and soft magnetic phases.

Figure 4 shows the 3-D FORC diagrams obtained by Eq. (1), and the contour plot of the 3-D FORC diagrams, in H_c and H_i coordinates, are shown in Figure 5. In the diagram of the sample with $T_f = 833$ K one can observe the presence of a narrow ridge centered around $H_c = 0$, that is the reversible component of the magnetization [13,21], and only one peak corresponding to irreversible component, at H_c around 45 Oe. It is also possible to see the beginning of the formation of other phases, as a small tail in the higher coercivity region.

In the diagram of the sample at $T_f = 953$ K it is possible to see four separate peaks which correspond (from left to right) to the reversible magnetization of the

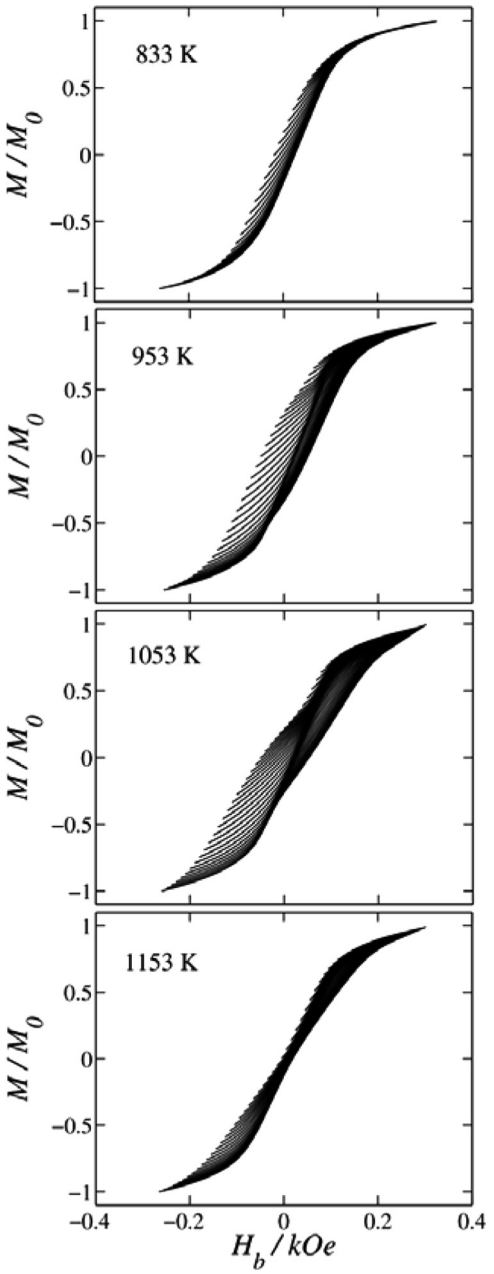

Figure 3. First order reversal curves (FORC) for the samples annealed up to different final temperatures ($T_f = 883$, 953, 1053, and 1153 K).

system, for H_c centered in zero, a soft magnetic phase in $H_c = 25$ Oe, Another peak at $H_c = 70$ Oe that has been associated to the coupling between the hard and soft phase [10] and the high coercivity phase, at $H_c = 105$ Oe, due to the Fe_7Co_3 nanoparticles. The presence of separated features in the FORC diagrams for a sample composed of coupled magnetic phases has been experimentally observed and modeled by

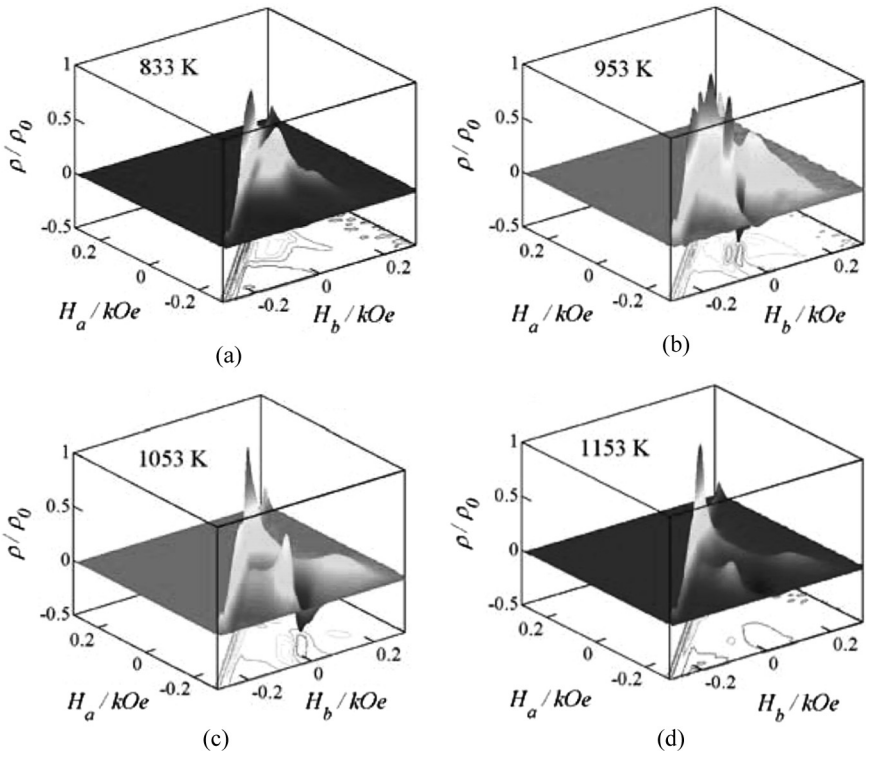

Figure 4. 3-D FORC diagrams obtained by Eq. (1), for the samples annealed up to different final temperatures ($T_f = 883$, 953, 1053, and 1153 K).

Chiriac *et al.* [10]. In their work they observed that the soft phase appear in the FORC diagrams with an interaction field H_i positive, while the hard magnetic phase and the coupling zone appear centered and with H_i negative. The position of each peak respect to H_c gives the effective coercivity of each phase.

The FORC diagram for the sample annealed at $T_f = 1053$ K shows roughly the same features observed for the sample treated at $T_f = 953$ K. However, the peaks appear more separated in this sample. The soft phase is more close to $H_c = 0$ Oe, centered in $H_c = 5$ Oe. The coupling is at $H_c = 95$ Oe, and the hard phase is centered at $H_c = 185$ Oe. The negative region is less pronounced and broader. For the sample annealed at $T_f = 1153$ K, the peaks corresponding to different phases lose intensity. The low coercivity phase is at 4 Oe, the hard phase is at $H_c = 180$ Oe and the coupling phase is at $H_c = 77$ Oe.

FORC diagrams can also gives information about coercive field distribution and the ratio of the reversible and irreversible magnetization processes in the sample [13,21].

It is interesting to note that the reversible component of the magnetization (centered in $H_c = 0$) for all samples is higher than the irreversible component (the spots for $H_c > 0$). This is attributed to the fact that even after thermal treatment at high temperatures, the amount of material that remain in the amorphous state is substantially higher than the amount of Fe_7Co_3 nano-crystalline grains formed. This is in agreement with the analysis of the X-ray diffractions.

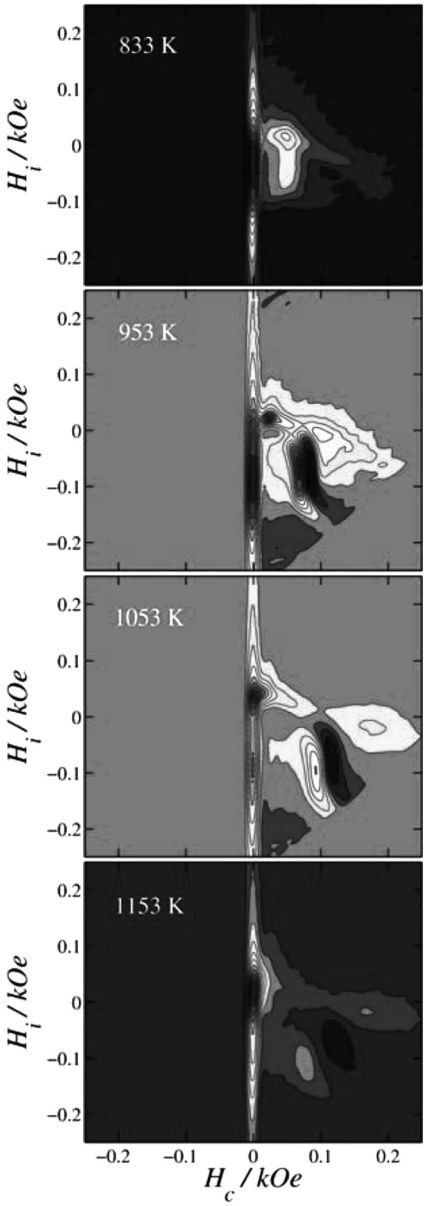

Figure 5. FORC diagrams, i.e., the contour plot of the 3-D graphs, in H_c and H_i coordinates.

The relative spread of the FORC diagrams along the H_i axis correspond to interparticle interactions, and it is worth to notice that the peaks which have been associated to the coupling between phases [10] appears as elongated narrow peaks centred at negative H_i axes.

Finally, the spread of FORC diagrams in the H_c axis is a direct measure of the increase of distribution of coercivities in the samples, which is a consequence of the increase of particle sizes and distributions with annealing.

Conclusion

Thermal annealing was used to generate structural modifications on an amorphous magnetic alloy, controlling the generation of magnetic nanoparticles and tuning the magnetic properties. From the analysis of structural and magnetic characterizations one can see that increasing the annealing final temperature, increasing the size of the Fe_7Co_3 nano-crystallites, the coercivity of a hard magnetic phase is increased. By means of FORC diagrams we have observed an increase in the separation of the coercivities of the different phases with T_f, and the coercivity values of each phase can be determined with precision. Finally, the FORC diagrams allow one to obtain a more complete characterization of complex systems, giving the coercivity distribution and the reversible and irreversible component of the magnetization, which are difficult to obtain from a simple hysteresis curve.

Acknowledgments

This work was supported by the Proyecto Fondecyt Postdoctorado (Grant No. 3100117), the Financiamiento Basal para Centros Científicos y Tecnológicos de Excelencia (CEDENNA), the Millennium Science Nucleus *Basic and Applied Magnetism* (Grant No. P06–022 F), and the Fondecyt (Grant No. 1080164).

References

[1] Vázquez, M. & Hernando, A. (1995). *Adv. Mater.*, *7*, 1021.
[2] Herzer, G. (1993). *Phys. Scripta.*, *T49*, 307.
[3] Hernando, A. & Kulik, T. (1994). *Phys. Rev. B.*, *49*, 7064.
[4] Randrianantoandro, N., Slawska-Waniewska, A., & Greneche, J. M. (1997). *Phys. Rev. B.*, *56*, 10797.
[5] Schmool, D. S., Garitaonandia, J. S., & Barandiarán, J. M. (1998). *Phys. Rev. B.*, *58*, 12159.
[6] Slawska-Waniewska, A., Roig, A., Molins, E., Greneche, J. M., & Zuberek, R. (1997). *J. Appl. Phys.*, *81*, 4652.
[7] Slawska-Waniewska, A., Gutowski, M., Lachowicz, H. K., Kulik, T., & Matyja, H. (1992). *Phys. Rev. B.*, *46*, 14594.
[8] Dumas, R. K., Li, Ch.-P, Roshchin, I. V., Schuller, I. K., & Liu, K. (2007). Magnetic fingerprints of sub-100 nm Fe dots. *Phys. Rev. B.*, *75*, 134405.
[9] Pike, C. & Fernandez, A. (1999). An investigation of magnetic reversal in submicron-scale Co dots using first order reversal curve diagrams. *J. Appl. Phys.*, *85*, 9.
[10] Chiriac, H., Lupu, N., Stoleriu, L., Postolache, P., & Stancu, A. (2007). Experimental and micromagnetic first-order reversal curves analysis in NdFeB-based bulk "exchange spring" type permanent magnets. *J. Magn. Magn. Mater.*, *316*, 177–180.
[11] Pike, C. R., Ross, C. A., Scalettar, R. T., & Zimanyi, G. (2005). First-order reversal curve diagram analysis of a perpendicular nickel nanopillar array. *Phys. Rev. B.*, *71*, 134407.
[12] Lavín, R., Denardin, J. C., Escrig, J., Altbir, D., Cortés, A., & Gómez, H. (2008). Characterization of Nanowire Arrays Using First Order Reversal Curves. *IEEE. Trans. Magn.*, *44*, 2808.
[13] Béron, F., Ménard, D., & Yelon, A. (2008). First-order reversal curve diagrams of magnetic entities with mean interaction field: A physical analysis perspective. *J. Appl. Phys.*, *103*, 07D908.
[14] Pike, C., Roberts, A. P., & Verosub, K. L. (1999). Characterizing interactions in fine magnetic particle systems using first order reversal curves. *J. Appl. Phys.*, *85*, 6660.
[15] Kissinger, H. E. (1956). *Journal of Research of the National Bureau of Standars.*, *57*, 4.

[16] Wesley, W. M. Wendlandt, Thermal Analysis, Vol. 10, 3rd ed.
[17] Cullity, B. D. (1978). Elements of X-Ray Diffraction: Addison-Wesley Publishing Company: 2nd ed.
[18] Zhengfung, Q. (1985). *Transactions of the Metals Heat Treatment.*, *2*, 9–19.
[19] Baker, I. (1997). Thayer School of Engineering Dartmouth College, NH. USA. ICDD Grant-in-Aid.
[20] Bertotti, G. (1998). *Hysteresis in Magnetism*, Academic Press: San Diego.
[21] Pike, C. R. (2003). First-order reversal-curve diagrams and reversible magnetization. *Phys. Rev. B.*, *68*, 104424.
[22] Spinu, L., Stancu, A., Radu, C., Li, F., & Wiley, J. B. (2004). Method for Magnetic Characterization of Nanowire Structures. *IEEE Trans. Magn.*, *40*, 2116–2118.
[23] Hansen, M. F., Vecchio, K. S., Parker, F. T., Spada, F. E., Berkowitz, A. E. (2003). Exchange-spring permanent magnet particles produced by spark-erosion. *Appl. Phys. Lett.*, *82*, 10.
[24] Lu, M. H., Song, T., Zhou, T. J., Wang, J. P., Piramanayagam, S. N., Ma, W. W., & Gong, H. (2004). FePt and Fe nanocomposite by annealing self-assembled FePt nanoparticles. *J. Appl. Phys.*, *95*, 11.
[25] Huang, M. Q., Hsu, Y. N., McHenry, M. E., & Laughlin, D. E. (2001). Soft Magnetic Properties of Nanocrystalline Amorphous HITPERM Films and Multilayers. *IEEE Trans. Magn.*, *37*, 4.
[26] Zhao, X. G., Zhang, Z. D., Cui, B. Z., Ren, W. J., Liu, W., & Geng, D. Y. (2003). Structure and magnetic properties of nanostructured $Pr_{1-x}Gd_xCo_5$ ($x = 0$–1) powders prepared by mechanical alloying. *J. Appl. Phys.*, *93*, 8125.
[27] Okumura, H., Um, C. Y., Chu, S. Y., McHenry, M. E., Laughlin, D. E., & Kos, A. B. (2004). Structure and Magnetic Switching of Thin-Film a-HITPERM/SiO2 Soft Magnetic Multilayers. *IEEE Trans. Magn.*, *40*, 4.
[28] Mao, X., Han, Z., Xu, F., Gao, W., Gu, B., & Du, Y. (2005). The effect of thermal treatment on the magnetic properties of Ge-doped FeNbB alloys. *Appl. Phys. A.*, *81*, 839–842.
[29] Blázquez, J. S., Franco, V., Conde, A., Gibbs, M. R. J., Davies, H. A., & Wang, Z. C. (2002). The evolution of magnetostriction and coercivity with temperature in the early stages of nanocrystallisation in FeCoNbB(Cu) alloys. *J. Magn. Magn. Mater.*, *250*, 260–266.
[30] Bennett, L. H. & Torre, E. D. (2005). Analysis of wasp-waist hysteresis loops. *J. Appl. Phys.*, *97*, 10E502.
[31] Kahler, G. R., Bennett, L. H., & Torre, E. D. (2006). Coercivity and the critical switching field. *Physica B.*, *372*, 1–4.
[32] Sementsov, D. I., & Shutyi, A. M. (2004). Hysteresis Loops of a Periodic Multilayered Structure with Antiferromagnetic Coupling. *Crystallography Reports.*, *49*, 6.